International Journal of Engineering, Mathematical and Physical Sciences
ISSN: 2517-9934
Vol:10, No:12, 2016

An Implicit Methodology for the Numerical Modeling of Locally Inextensible Membranes

Aymen Laadhari

***Abstract*—**We present in this paper a fully implicit finite element method tailored for the numerical modeling of inextensible fluidic membranes in a surrounding Newtonian fluid. We consider a highly simplified version of the Canham-Helfrich model for phospholipid membranes, in which the bending force and spontaneous curvature are disregarded. The coupled problem is formulated in a fully Eulerian framework and the membrane motion is tracked using the level set method. The resulting nonlinear problem is solved by a Newton-Raphson strategy, featuring a quadratic convergence behavior. A monolithic solver is implemented, and we report several numerical experiments aimed at model validation and illustrating the accuracy of the proposed method. We show that stability is maintained for significantly larger time steps with respect to an explicit decoupling method.

***Keywords*—**Finite element method, Newton method, level set, Navier-Stokes, inextensible membrane, liquid drop.

I. Introduction

THIS work is concerned with the development and numerical implementation of a fully implicit method suitable for the modeling of the dynamics of single fluidic membranes in a surrounding Newtonian fluid. Fluidic membranes such as phospholipid membranes are abundant in many real life and industrial applications [18]. They have a complex assembly of phospholipid bilayers composed by amphiphilic molecules [26]. In particular, red blood cells, referred to as RBCs, and vesicles (biomimetic membranes) are of great interest by several scientific communities [4], [16], [24]. We consider a highly simplified version of the Canham-Helfrich model [6], [7], [9] introduced to model the mechanical properties of RBCs and more generally biological membranes. In the present work, the simplified membrane model disregards the bending force and the spontaneous curvature of the membrane but accounts for the inhomogeneous surface tension, see [17]. This preliminary work can be also suitable to model liquid drops and constitutes one step in our attempt to study the deformations of vesicles and RBCs under the bending energy.

The aforementioned problem was widely studied in the literature and several methodologies have been developed, see e.g. [2]–[4], [11], [12], [15], [24]. However, the most existing works have used fully explicit decoupling strategies for the fluid problem and the shape deformation, leading a severe stability condition. Only few works have proposed semi-implicit approaches such as [2] for the vesicle problem and [10] for the capillary problem with homogeneous surface tension coefficient. The fully implicit time discretization methods are conditionally stable and enable to overcome the severe restrictions related to the setting of time step. In this paper, we describe a fully implicit strategy by combining the level set and Newton methods to solve the nonlinear coupling between the fluid problem and the membrane mechanics endowed with the simplified Helfrich force. We focus on the two-dimensional case, although the three-dimensional formulation of the tangent problem does not introduce any changes or additional complexities.

A. Laadhari is with the Department of Information Technology and Electrical Engineering, Swiss Federal Institute of Technology Zürich (Eidgenössische Technische Hochschule Zürich), CH-8092 Zürich, Switzerland. E-mail: laadhari@vision.ee.ethz.ch.

Manuscript received September 30, 2016.

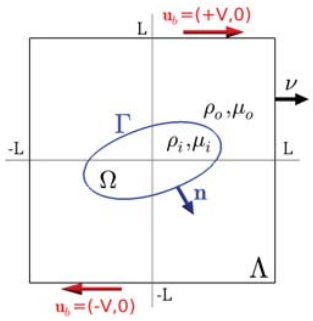

Fig. 1 A sketch for the membrane Γ with a reduced area $\Xi_{2d} = 0.6$ and embedded in a square computational domain Λ of size 2L

The paper is organized as follows. In Section II, we introduce some required notations and we provide a mathematical setting for the coupled nonlinear problem. Section III presents the semidiscrete finite element approximation and describes the Newton strategy. A set of numerical examples showing the main features and the accuracy of the methodology are described in Section IV. The conclusions and forthcoming extensions are summarized in Section V. Details on the linearization are provided in appendix A.

II. Mathematical Setting

A. Notations

Let $T > 0$ represent the period of the computations. For any time $t \in (0, T)$, let $\Omega(t) \subset \mathbb{R}^2$ design the intracellular domain (dense suspension of hemoglobin for RBCs), and having a Lipschitz continuous boundary $\Gamma(t) = \partial\Omega(t)$. The membrane is embedded in a larger computational domain Λ (plasma for RBCs) such that $\Gamma(t) \cap \partial\Lambda = \emptyset$ for all $t \in (0, T)$, see Fig. 1. Let $\boldsymbol{n}$ and $\boldsymbol{\nu}$ denote the unit outward normal vector on the membrane $\Gamma(t)$ and the external boundary $\partial\Lambda$, respectively. From now, the explicit dependence of Ω and Γ from t will

be understood. We give two surface operators needed along this paper. Let $\varkappa$ be a scalar function, $\boldsymbol{v}$ be a vector field and $\mathbf{Id}$ be the identity tensor. Let $\otimes$ denote the tensorial product between vectors. The surface gradient and surface divergence operators are respectively expressed as:

$$\boldsymbol{\nabla}_s \varkappa = (\mathbf{Id} - \boldsymbol{n} \otimes \boldsymbol{n})\ \boldsymbol{\nabla} \varkappa \ \text{ and } \ \operatorname{div}_s \boldsymbol{v} = \operatorname{tr}(\boldsymbol{\nabla}_s \boldsymbol{v}).$$

B. Simplified Membrane Model

To describe the mechanical properties of phospholipid membranes, Canham [6] and Helfrich [7], [9] introduced independently a mathematical model that formulates the physical properties of the cell membrane with respect to the curvature. Here, we use a highly simplified version of this energy, in which we disregard the bending and the asymmetry effect of the membrane and its surrounding environment. However, we only preserve the inhomogeneities within the structure of the membrane [17].

The deformations of the fluidic membranes are subject to specific constraints [18]. First, the incompressibility condition of the intracellular and extracellular domains results from the impermeability of the membrane. Second, the membrane is not allowed to stretch and should preserve consequently its circumference (surface area in 3D) during the dynamics that represents to the local inextensibility which corresponds to a zero surface divergence of the velocity [16], [25]. Hence, we introduce a local Lagrange multiplier λ that represents the membrane tension and depends on the position on the membrane (analogous to the pressure that corresponds to the fluid incompressibility constraint). Accordingly, we consider the constrained space of admissible velocities:

$$\Big\{ \boldsymbol{u} : \quad \operatorname{div} \boldsymbol{u} = 0 \text{ in } \Lambda \quad \text{and} \quad \operatorname{div}_s \boldsymbol{u} = 0 \text{ on } \Gamma \Big\}.$$

Using a shape differentiation methodology [13], the corresponding force reads:

$$\boldsymbol{F}_\Gamma = \lambda H \boldsymbol{n} - \boldsymbol{\nabla}_s \lambda \quad \text{ on } (0,T) \times \Gamma. \tag{1}$$

The force $\boldsymbol{F}_\Gamma$ corresponds to the jump of the normal stresses across the membrane and gives rise to two components involving the space varying surface tension λ. The first term is similar to the capillary forces engendered by the surface tension for drops and bubbles, while the second term is tangential to the membrane and corresponds to the movement of particles on the membrane without affecting its shape; that is known as the Marangoni effect.

C. Level Set Method

We follow the membrane motion in an Eulerian framework in such a way that the evolving membrane represents the iso-value zero of a level set function [21]:

$$\Gamma(t) = \Big\{ (t, \boldsymbol{x}) \in (0,T) \times \Lambda : \varphi(t, \boldsymbol{x}) = 0 \Big\}.$$

The intracellular domain Ω corresponds to the set $\varphi < 0$. For any $t \in (0,T)$, a time-dependant initial value partial differential equation describes the motion of Γ:

$$\frac{\partial \varphi}{\partial t} + \boldsymbol{u} \cdot \boldsymbol{\nabla} \varphi = 0, \qquad \text{in } (0,T) \times \Lambda.$$

This problem is initialized with a suitable distance function φ_0 to $\Gamma(0)$:

$$\varphi_0(\boldsymbol{x}) = \begin{cases} \inf\limits_{\boldsymbol{y} \in \Gamma(0)} |\boldsymbol{y} - \boldsymbol{x}| \ \text{ if } \boldsymbol{x} \notin \Omega(0), \\ -\inf\limits_{\boldsymbol{y} \in \Gamma(0)} |\boldsymbol{y} - \boldsymbol{x}| \ \text{ otherwise.} \end{cases}$$

The mean curvature H is introduced as the sum of the principle curvatures on the membrane. All geometrical quantities, e.g. $\boldsymbol{n}$ and H, are naturally encoded in terms of φ and are consequently extended to the entire Λ. We have

$$\boldsymbol{n} = \frac{\boldsymbol{\nabla} \varphi}{|\boldsymbol{\nabla} \varphi|} \quad \text{ and } \quad H = \operatorname{div}_s \boldsymbol{n} = \operatorname{div} \boldsymbol{n}.$$

It is common to introduce a regularization approach that avoids using meshes that fit the membrane deformation. Let us introduce a regularization parameter ε proportional to the mesh size h. The regularized Heaviside function $\mathscr{H}$, Dirac measure δ_Γ and sign function $\mathcal{S}$ in a banded strip of width 2ε are respectively given by:

$$\mathscr{H}_\varepsilon(\varphi) = \begin{cases} 0, & \text{when } \varphi < -\varepsilon \\ \dfrac{1}{2}\left(1 + \dfrac{\varphi}{\varepsilon} + \dfrac{1}{\pi} \sin\left(\dfrac{\pi \varphi}{\varepsilon}\right)\right), & \text{when } |\varphi| \leqslant \varepsilon, \\ 1, & \text{otherwise} \end{cases}$$

$$\delta_\varepsilon(\varphi) = \frac{\mathrm{d}\mathscr{H}_\varepsilon}{\mathrm{d}\varphi}(\varphi) \quad \text{and} \quad \mathcal{S}_\varepsilon(\varphi) = 2\mathscr{H}_\varepsilon(\varphi) - 1.$$

For any given function $\xi(\cdot)$ defined on Γ, an extension $\tilde{\xi}(\cdot)$ to the entire domain Λ is required, and the surface integrals are approximated by:

$$\int_\Gamma \xi(\boldsymbol{x})\ d\boldsymbol{s} = \int_\Lambda |\boldsymbol{\nabla} \varphi|\ \delta_\Gamma\, \tilde{\xi}(\boldsymbol{x})\, d\boldsymbol{x} \approx \int_\Lambda |\boldsymbol{\nabla} \varphi|\ \delta_\varepsilon\left(\varphi\right)\ \tilde{\xi}(\boldsymbol{x})\, d\boldsymbol{x}.$$

The signed distance property is lost after the advection of the level set, resulting in bad scenarios where the gradient becomes too large or too small near Γ. That can deteriorate the accurate computations over Γ. A "redistancing problem" commonly helps to re-establish the signed distance property [21]. At any time $t \in (0,T)$, let τ be a pseudo-time variable. We shall solve until convergence the problem:

$$\begin{cases} \dfrac{\partial \phi}{\partial \tau}(\tau, \cdot; t) + \mathcal{S}_\varepsilon(\varphi(t, \cdot))\big(\,|\boldsymbol{\nabla} \phi(\tau, \cdot; t)| - 1\big) = \zeta(\tau, \cdot; t), \\ \phi(0, \cdot; t) = \varphi(t, \cdot), \end{cases}$$

where $\mathcal{S}_\varepsilon(\varphi)$ enables to impose a zero-displacement on the membrane, and $\zeta(\tau, \cdot; t)$ is an explicit Lagrange multiplier which acts as a constraint enforcing the unphysical shifting of the membrane during the redistancing process. We follow the redistancing method described in [16]. When the convergence is achieved, the level set function $\varphi(t, \cdot)$ is updated with the solution $\phi(\infty, \cdot; t)$. At the numerical level, we use a first order combined characteristic and finite difference discretization method to approximate the advection term in the redistancing problem. In addition, we consider the Gauss-Lobatto quadrature formula which guaranties further stability for the characteristics method [5], [23].

D. Statement of the Nonlinear Coupled Problem

Let us consider a Newtonian fluid in both sides of the fluidic membrane Γ. We assume a constant density ρ_i for the inner fluid and ρ_o for the ambient fluid, see Fig. 1. Analogously, we introduce the constant viscosities μ_i and μ_o. Let 1_Ω represent the characteristic function of Ω. The global density function is given with respect to the level set function by $\rho(\varphi) = \rho_i 1_{\varphi<0} + \rho_o 1_{\varphi\geqslant 0}$. Similarly, the global viscosity function $\mu(\varphi)$ is introduced. Let $\boldsymbol{\sigma}(\boldsymbol{u}, p, \varphi) = 2\mu(\varphi)\mathbf{D}(\boldsymbol{u}) - p\boldsymbol{I}$ and $\mathbf{D}(\boldsymbol{u}) = (\nabla \boldsymbol{u} + \nabla \boldsymbol{u}^T)/2$ be the fluid Cauchy stress tensor and the strain tensor, respectively.

We consider two complementary subsets Σ_D and Σ_N of the boundary $\partial\Lambda$ on which essential or natural boundary conditions are assigned, respectively. Let $\boldsymbol{u}_b$ represent the velocity field on Σ_D and φ_b be the level set on the upstream boundary $\Sigma_- = \left\{\boldsymbol{x} \in \partial\Lambda \,:\, \boldsymbol{u}\cdot\boldsymbol{\nu}(\boldsymbol{x}) < 0\right\}$. We introduce the following spaces of admissible velocities, pressures, membrane tension and level set:

$$\mathbb{V}(\boldsymbol{u}_b) = \left\{\boldsymbol{v} \in \left(H^1(\Omega)\right)^d \,:\, \boldsymbol{v} = \boldsymbol{u}_b \ \text{ on } \Gamma_D\right\},$$
$$\mathbb{Q} = \left\{q \in L^2(\Omega) \,:\, \int_\Omega q\, d\boldsymbol{x} = 0\right\},\ \mathbb{W} = H^{-1/2}(\Gamma)$$
$$\text{and } \mathbb{X}(\varphi_b) = \left\{\psi \in W^{1,\infty}(\Lambda) \,:\, \psi = \varphi_b \ \text{ on } \Sigma_-\right\}.$$

Let us denote by $[\boldsymbol{u}]^+_- = \boldsymbol{u}_+ - \boldsymbol{u}_-$ and $[\boldsymbol{\sigma n}]^+_- = \boldsymbol{\sigma}_+\boldsymbol{n} - \boldsymbol{\sigma}_-\boldsymbol{n}$ the jumps in the velocity and normal stress across the membrane, respectively. Collecting the elements above, we end with the following coupled model describing the iteration between the membrane and the surrounding fluid:

$\mathscr{P}$: find the velocity $\boldsymbol{u}$, pressure p, membrane tension λ and level set φ such that

$$\rho(\varphi)\left(\frac{\partial \boldsymbol{u}}{\partial t} + \boldsymbol{u}.\nabla\boldsymbol{u}\right) - \mathbf{div}\,\boldsymbol{\sigma}(\boldsymbol{u}, p, \varphi) = \mathbf{0} \ \text{ in } (0,T)\times(\Lambda\backslash\Gamma),$$
$$\text{div}\ \boldsymbol{u} = 0 \ \text{ in } (0,T)\times\Lambda$$
$$\text{div}_s\ \boldsymbol{u} = 0 \ \text{ on } (0,T)\times\Gamma$$
$$[\boldsymbol{u}]^+_- = \mathbf{0} \ \text{ on } (0,T)\times\Gamma$$
$$[\boldsymbol{\sigma n}]^+_- = \boldsymbol{\nabla}_s\lambda - \lambda H\boldsymbol{n} \ \text{ on } (0,T)\times\Gamma$$
$$\frac{\partial\varphi}{\partial t} + \boldsymbol{u}.\nabla\varphi = 0 \ \text{ in } (0,T)\times\Lambda$$
$$\varphi = \varphi_b, \ \text{ on } \ (0,T)\times\Sigma_-$$
$$\boldsymbol{u} = \boldsymbol{u}_b, \ \text{ on } \ (0,T)\times\Sigma_D$$
$$\boldsymbol{\sigma\nu} = \mathbf{0} \ \text{ on } \ (0,T)\times\Sigma_N.$$

Initial data are given by $\boldsymbol{u}(0) = \boldsymbol{u}_0$ and $\varphi(0) = \varphi_0$, and the shape of the membrane Γ is assumed sufficiently regular during the dynamics. The normal stress discontinuity across the membrane is obtained using the Green transformations and is calibrated by the mean curvature and the membrane tension.

We thereafter proceed with the non-dimensionalization of problem $\mathscr{P}$. Let U and D represent the maximum instantaneous velocity on Σ_D and the diameter of a circle having the same perimeter as the membrane, respectively. We introduce the Reynolds number $Re = \rho U D \mu_i^{-1}$ which compares the membrane forces to the viscous effects. In addition, the cell confinement is given by $\varsigma = D/(2L)$, see Fig. 1. The viscosity ratio $\mu^\star = \mu_o/\mu_i$ expresses the extracellular viscosity with respect to the intracellular viscosity. Thus, the dimensionless and regularized viscosity function reads:

$$\mu_\varepsilon(\varphi) = \mu^\star \mathscr{H}_\varepsilon(\varphi) + 1 - \mathscr{H}_\varepsilon(\varphi). \tag{2}$$

In addition, we introduce two dimensionless shape parameters that measure the cell deflation: the reduced area and the excess length. They are given by the following expressions:

$$\Xi_{2d} = 4\pi\frac{|\Omega(0)|}{|\Gamma(0)|} \quad \text{and} \quad \Delta_{2d} = |\Gamma(0)|\sqrt{\frac{2\pi}{|\Omega(0)|}} - 2\pi.$$

The reduced area Ξ_{2d} compares the enclosed area $|\Omega|$ to the area of a circle having the same perimeter $|\Gamma|$. The excess length Δ_{2d} measures the shape difference with respect to the fully circular shape.

In what follows, all the quantities are dimensionless and we keep using the same previous notations for the new non-dimensionalized variables for ease of exposition. Moreover, we suppose without loss of generality that the fluid has the same density inside and outside the membrane, i.e. $\rho_i = \rho_o$. Indeed, including different densities is very easy in such an Eulerian framework (similarly to (2)). This assumption will be used in the numerical examples in Section IV.

III. Numerical Approximation

A. Time Discretization

Let us divide $[0,T]$ into N subintervals $[t^n, t^{n+1})$, $n = 0,\ldots,N-1$ of uniform time steps Δt. For any $n \geqslant 1$, the unknowns $\boldsymbol{u}^n$, p^n, λ^n and φ^n at time step n are computed iteratively. The surface divergence operator is approximated at t^n in such a way that $\text{div}_s^n\,\boldsymbol{v}$ stands for $(\mathbf{Id} - \boldsymbol{n}^n\otimes\boldsymbol{n}^n) : \boldsymbol{\nabla v}$, in which $\boldsymbol{n}^n$ is an approximation of the normal vector $\boldsymbol{n}$ at t^n. Analogously, the surface gradient operator $\boldsymbol{\nabla}_s^n$ is introduced.

To write the variational formulation, the problem $\mathscr{P}$ is tested with suitable test functions and we shall integrate the momentum equation in both Ω and $\Lambda\backslash\overline{\Omega}$ separately. The Green formulation for closed surface integrals is subsequently used such that:

$$\int_{\Gamma^n}\boldsymbol{\nabla}_s^n\lambda^n\cdot\boldsymbol{v} + \int_{\Gamma^n}\lambda^n\,\text{div}_s^n\,\boldsymbol{v} - \int_{\Gamma^n}\lambda^n\,\text{div}(\boldsymbol{n}^n)\boldsymbol{n}^n\cdot\boldsymbol{v} = 0.$$

Therefore, the semi-discretized problem $\mathscr{P}$ reads:

$\mathscr{P}^n$: find $\boldsymbol{u}^n$, p^n, λ^n and φ^n such that

$$Re\int_\Lambda\left(\frac{\boldsymbol{u}^n - \boldsymbol{u}^{n-1}}{\Delta t} + \boldsymbol{u}^n.\boldsymbol{\nabla}\boldsymbol{u}^n\right)\cdot\boldsymbol{v} - \int_{\Gamma^n}\lambda^n\,\text{div}_s^n\,\boldsymbol{v}$$
$$+\int_\Lambda 2\mu_\varepsilon(\varphi^n)\,\mathbf{D}(\boldsymbol{u}^n) : \mathbf{D}(\boldsymbol{v}) - \int_\Lambda p^n\,\text{div}\ \boldsymbol{v} = 0, \tag{3}$$
$$\int_\Lambda q\ \text{div}\ \boldsymbol{u}^n = 0, \tag{4}$$
$$\int_{\Gamma^n}\eta\,\text{div}_s^n\,\boldsymbol{u}^n = 0, \tag{5}$$
$$\int_\Lambda\frac{\varphi^n - \varphi^{n-1}}{\Delta t}\psi + \int_\Lambda(\boldsymbol{u}^n\cdot\nabla\varphi^n)\,\psi = 0, \tag{6}$$

for all $\boldsymbol{v} \in \mathbb{V}(0)$, $q \in \mathbb{Q}$, $\eta \in \mathbb{W}$ and $\psi \in \mathbb{X}(0)$. Let us denote by $\boldsymbol{\chi}$ the global vector of unknowns $(\boldsymbol{u}, p, \lambda, \varphi)$,

and let $\Psi = (\boldsymbol{v}, q, \eta, \psi)$ be the corresponding test function. All surface integrals in $\mathscr{P}^n$ are transformed into integrals over Λ as aforementioned in Section II-C. We introduce the operator $\mathscr{R}(\boldsymbol{\chi})$ as the global residual vector corresponding to the regularized problem. Let $\langle .,. \rangle$ stand for the duality product. The problem (3)-(6) reads in a compact form:

find $\boldsymbol{\chi}^n$ *such that*

$$\langle \mathscr{R}(\boldsymbol{\chi}^n), \Psi \rangle = \Big(\langle \mathscr{R}_{\boldsymbol{\chi}}(\boldsymbol{\chi}^n), \boldsymbol{v} \rangle_{\mathbb{V}(0)',\mathbb{V}(0)}, \langle \mathscr{R}_p(\boldsymbol{u}^n), q \rangle_{\mathbb{Q}',\mathbb{Q}}, \langle \mathscr{R}_\lambda(\boldsymbol{u}^n), \xi \rangle_{\mathbb{W}',\mathbb{W}}, \langle \mathscr{R}_{\boldsymbol{u},\varphi}(\boldsymbol{u}^n, \varphi^n), \psi \rangle_{\mathbb{X}(0)',\mathbb{X}(0)} \Big)^T = \mathbf{0}, \ \forall \Psi.$$

B. Newton-Raphson Method

The Newton-Raphson method reduces the nonlinear problem $\mathscr{R}(\boldsymbol{\chi}^n) = \mathbf{0}$ (3)-(6) into a sequence of linear sub-problems [14]. Given the starting value $\boldsymbol{\chi}_0^n = \boldsymbol{\chi}^n$, the algorithm computes iteratively the solution $\boldsymbol{\chi}_k^n$ with $k > 0$. Indeed, the velocity, pressure, surface tension and level set increments $\delta\boldsymbol{\chi}_k^n = (\delta\boldsymbol{u}_k^n; \delta p_k^n, \delta\lambda_k^n, \delta\varphi_k^n)$ are computed at each sub-iteration $k \geqslant 1$ such that:

$$\langle D\mathscr{R}(\boldsymbol{\chi}_k^n)[\delta\boldsymbol{\chi}_k^n], \boldsymbol{v} \rangle = -\langle \mathscr{R}(\boldsymbol{\chi}_k^n), \boldsymbol{v} \rangle, \tag{7}$$

where $D\mathscr{R}(\boldsymbol{\chi})[\delta\boldsymbol{\chi}]$ represents the directional derivative of $\mathscr{R}$ in the direction $\delta\boldsymbol{\chi}$. The solution is then explicitly updated by

$$\boldsymbol{\chi}_{k+1}^n = \boldsymbol{\chi}_k^n + \delta\boldsymbol{\chi}_k^n.$$

Since the Newton algorithm has only local convergence properties, we use a second order extrapolation of the solution of previous time steps to assign the starting values $\boldsymbol{\chi}_0^n$. The method is applied recursively until the stopping criteria based on the computation of the global residual is satisfied. At the numerical level, a tolerance equal to 10^{-8} is considered.

To simplify the derivation of the tangent problem, the regularized problem $\mathscr{P}^n$ is simplified based on the signed distance property obtained by solving until convergence the redistancing problem. Accordingly, the signed distance assumption $|\boldsymbol{\nabla}\varphi^n| = 1$ everywhere enables to simplify the Jacobian matrix, reducing then the computational cost. However, we emphasize that the expected quadratic convergence of the Newton strategy may be significantly deteriorated if the redistancing problem is not solved until convergence. In fact, the Jacobian system becomes inexact and the missing terms corresponding to $|\boldsymbol{\nabla}\varphi| \neq 1$ should be considered to re-establish the second-order convergence behavior.

For ease of exposition, we will drop the superscript n whenever it is clear from the context, and we rather write k as a superscript. We introduce the following multi-linear forms:

$$a(\boldsymbol{u}, \boldsymbol{v}; w) = \int_\Lambda 2w\mathbf{D}(\boldsymbol{u}) : \mathbf{D}(\boldsymbol{v}); \ b(\boldsymbol{u}, q; \mathbf{T}) = -\int_\Lambda q\mathbf{T} : \boldsymbol{\nabla}\boldsymbol{u};$$
$$c(\boldsymbol{u}, \boldsymbol{v}; \boldsymbol{w}) = \int_\Lambda \Big((\boldsymbol{u}\cdot\boldsymbol{\nabla})\boldsymbol{w} + (\boldsymbol{w}\cdot\boldsymbol{\nabla})\boldsymbol{u} \Big) \cdot \boldsymbol{v};$$
$$d(\varphi, \boldsymbol{v}; w) = \int_\Lambda w\boldsymbol{\nabla}\varphi \cdot \boldsymbol{v}; h(\varphi, \boldsymbol{v}; w, \boldsymbol{w}) = a(\boldsymbol{w}, \boldsymbol{v}; w\varphi);$$
$$m(\boldsymbol{u}, \boldsymbol{v}) = \int_\Lambda \boldsymbol{u}\cdot\boldsymbol{v}; g(\varphi, \boldsymbol{v}; \boldsymbol{w}) = \int_\Lambda \varphi\boldsymbol{v}\cdot\boldsymbol{w};$$
$$e(\varphi, \psi; w) = \int_\Lambda w\,\varphi\psi; \ k(\varphi, \boldsymbol{v}; \boldsymbol{w}, \mathbf{P}) = \int_\Lambda (\boldsymbol{w}\cdot\boldsymbol{\nabla}\varphi)(\mathbf{P} : \boldsymbol{\nabla}\boldsymbol{v});$$
$$l(\varphi, \boldsymbol{v}; \boldsymbol{w}) = \int_\Lambda \big(\boldsymbol{\nabla}\varphi \otimes \boldsymbol{w} + \boldsymbol{w} \otimes \boldsymbol{\nabla}\varphi\big) : \boldsymbol{\nabla}\boldsymbol{v};$$
$$i(\varphi, \psi; \boldsymbol{w}) = \int_\Lambda \psi\boldsymbol{w}\cdot\boldsymbol{\nabla}\varphi; \ j(\varphi, \psi; \boldsymbol{w}, \tilde{\boldsymbol{w}}) = l(\varphi, \boldsymbol{w}; \psi\tilde{\boldsymbol{w}});$$

defined for all $\boldsymbol{u}, \boldsymbol{v}, \boldsymbol{w}, \tilde{\boldsymbol{w}} \in \mathbb{V}$; $q \in \mathbb{Q}$; $\varphi, \psi \in \mathbb{X}$; $w \in L^\infty(\Lambda)$ and $\mathbf{P} \in (L^\infty(\Lambda))^{2\times 2}$.

The residuals of the coupled system (3)-(6) are given by:

$$\begin{aligned}
\langle \mathscr{R}_{\boldsymbol{\chi}}(\boldsymbol{\chi}^k), \boldsymbol{v} \rangle_{\mathbb{V}(\mathbf{0})',\mathbb{V}(\mathbf{0})} &= \frac{\mathrm{Re}}{\Delta t} m\Big(\boldsymbol{u}^k - \boldsymbol{u}^{n-1}, \boldsymbol{v}\Big) \\
&+ \frac{\mathrm{Re}}{2} c\Big(\boldsymbol{u}^k, \boldsymbol{v}; \boldsymbol{u}^k\Big) + a\Big(\boldsymbol{u}^k, \boldsymbol{v}; \mu_\varepsilon(\varphi^k)\Big) + b\Big(\boldsymbol{v}, p^k; \mathbf{Id}\Big) \\
&+ b\Big(\boldsymbol{v}, \lambda^k; \delta_\varepsilon(\varphi^k)\Big(\mathbf{Id} - \boldsymbol{\nabla}\varphi^k \otimes \boldsymbol{\nabla}\varphi^k\Big)\Big), \\
\langle \mathscr{R}_p(\boldsymbol{u}^k), q \rangle_{\mathbb{Q}',\mathbb{Q}} &= b\big(\boldsymbol{u}^k, q; \mathbf{Id}\big), \\
\langle \mathscr{R}_\lambda(\boldsymbol{u}^k), \eta \rangle_{\mathbb{Q}',\mathbb{Q}} &= b\Big(\boldsymbol{u}^k, \eta; \delta_\varepsilon(\varphi^k)\big(\mathbf{Id} - \boldsymbol{\nabla}\varphi^k \otimes \boldsymbol{\nabla}\varphi^k\big)\Big), \\
\langle \mathscr{R}_\varphi(\varphi^k, \boldsymbol{u}^k), \psi \rangle_{\mathbb{X}(0)',\mathbb{X}(0)} &= \\
&\frac{1}{\Delta t} e\Big(\varphi^k - \varphi^{n-1}, \psi; 1\Big) + d\Big(\varphi^k, \boldsymbol{u}^k; \psi\Big).
\end{aligned}$$

Finally, the tangent problem corresponding to the system (3)-(6) is expressed in a compact form as:

Given $\boldsymbol{\chi}^k$*, find* $\delta\boldsymbol{\chi}^k = \big(\delta\boldsymbol{u}^k, \delta p^k, \delta\lambda^k, \delta\varphi^k\big)$ *such that*

$$\begin{aligned}
&\frac{\mathrm{Re}}{\Delta t} m\big(\delta\boldsymbol{u}^k, \boldsymbol{v}\big) + \mathrm{Re}\, c\big(\delta\boldsymbol{u}^k, \boldsymbol{v}; \boldsymbol{u}^k\big) + a\Big(\delta\boldsymbol{u}^k, \boldsymbol{v}; \mu_\varepsilon(\varphi^k)\Big) \\
&+ b\big(\boldsymbol{v}, \delta p^k; \mathbf{Id}\big) + b\Big(\boldsymbol{v}, \delta\lambda^k; \delta_\varepsilon(\varphi^k)\big(\mathbf{Id} - \boldsymbol{\nabla}\varphi^k \otimes \boldsymbol{\nabla}\varphi^k\big)\Big) \\
&+ b\Big(\boldsymbol{v}, \delta\varphi^k; \lambda^k\delta'_\varepsilon(\varphi^k)\big(\mathbf{Id} - \boldsymbol{\nabla}\varphi^k \otimes \boldsymbol{\nabla}\varphi^k\big)\Big) \\
&+ (\mu^\star - 1) h\big(\delta\varphi^k, \boldsymbol{v}; \delta_\varepsilon(\varphi^k), \boldsymbol{u}^k\big) + l\Big(\delta\varphi^k, \boldsymbol{v}; \lambda^k\delta_\varepsilon(\varphi^k)\boldsymbol{\nabla}\varphi^k\Big) \\
&= -\langle \mathscr{R}_{\boldsymbol{\chi}}(\boldsymbol{\chi}^k), \boldsymbol{v} \rangle_{\mathbb{V}(\mathbf{0})',\mathbb{V}(\mathbf{0})}, \qquad (8) \\
&b\big(\delta\boldsymbol{u}^k, q; \mathbf{Id}\big) = -\langle \mathscr{R}_p(\boldsymbol{u}^k), q \rangle_{\mathbb{Q}',\mathbb{Q}}, \qquad (9) \\
&b\Big(\delta\boldsymbol{u}^k, \eta; \delta_\varepsilon(\varphi^k)\big(\mathbf{Id} - \boldsymbol{\nabla}\varphi^k \otimes \boldsymbol{\nabla}\varphi^k\big)\Big) \\
&- e\Big(\delta\varphi^k, \eta; \delta'_\varepsilon(\varphi^k)\ \big(\mathbf{Id} - \boldsymbol{\nabla}\varphi^k \otimes \boldsymbol{\nabla}\varphi^k\big) : \boldsymbol{\nabla}\boldsymbol{u}^k\Big) \\
&+ j\Big(\delta\varphi^k, \eta; \boldsymbol{u}^k, \delta_\varepsilon(\varphi^k)\boldsymbol{\nabla}\varphi^k\Big) = -\langle \mathscr{R}_\lambda(\boldsymbol{u}^k), \eta \rangle_{\mathbb{Q}',\mathbb{Q}}, \qquad (10) \\
&\frac{1}{\Delta t} e\big(\delta\varphi^k, \psi; 1\big) + i\Big(\delta\varphi^k, \psi; \boldsymbol{u}^k\Big) \\
&+ g\Big(\psi, \delta\boldsymbol{u}^k; \boldsymbol{\nabla}\varphi^k\Big) = -\langle \mathscr{R}_\varphi(\varphi^k, \boldsymbol{u}^k), \psi \rangle_{\mathbb{X}(0)',\mathbb{X}(0)}, \qquad (11)
\end{aligned}$$

for all test functions $\boldsymbol{v}$, q, η and ψ.

Regarding the finite element approximation, the Taylor-Hood finite element is considered for the velocity and pressure, while the Lagrange polynomials of degree 1 are used to approximate the surface tension and level set function [5]. At the implementation level, we only consider in the global matrix of the linear system the non-zero coefficients corresponding to the Lagrange multiplier λ in a small surrounding of Γ.

IV. Numerical Results

The present method has been implemented using the C++ library for scientific computing Rheolef [23].

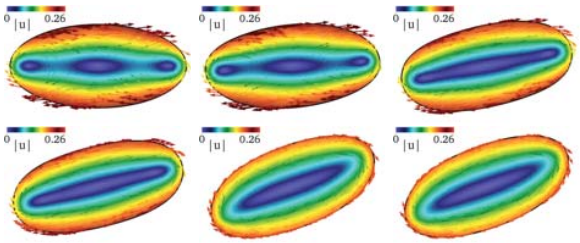

Fig. 2 Tank treading regime: Snapshots showing the dynamics of a membrane in simple shear flow (shape and velocity profile Ω) characterized by $\Xi_{2d} = 0.65$, $\mu^\star = 1$, $\mathrm{Re} = 10^{-3}$ and $\varsigma = 1/2$ at successive times $t \in \{0, 0.05, 0.15, 0.2, 1, 5\}$, respectively

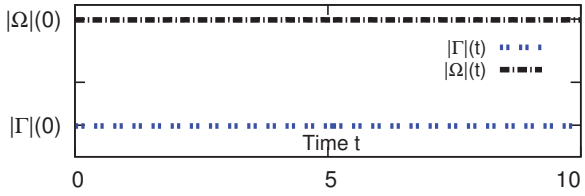

Fig. 3 Tank treading regime: Temporal evolution of the area and perimeter

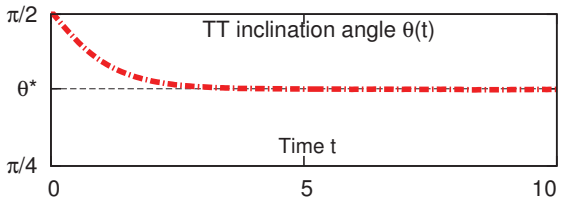

Fig. 4 Tank treading regime: Time evolution of the inclination angle

Distributed-memory parallelism relies on MPI [19]. Meshes have been generated using the software Gmsh [8]. The package Mumps [1], [20] is used for the factorization and as direct solver on distributed memory architectures. Numerical results are displayed graphically using the softwares Paraview [22] and Gnuplot [27].

A. Dynamics of Membranes under Simple Shear Flow

We consider a membrane having the reduced area $\Xi_{2d} = 0.65$ and placed in a square computational domain such that the confinement is $\varsigma = 1/2$. We consider a simple shear flow where the upper and lower boundaries move horizontally with opposite constant velocities $\mathbf{u}_b(\cdot, \pm L) = (\pm V, 0)$, see Fig. 1. A free-stress boundary condition $\boldsymbol{\sigma\nu} = \mathbf{0}$ is imposed on the remaining boundaries and the fluid is initially stationary.

We consider a Reynolds number $\mathrm{Re} = 10^{-3}$ characterizing vesicles in small capillaries [24]. Let us consider a small viscosity ratio $\mu^\star = 1$ between the interior and exterior fluid. The membrane undergoes the so-called tank-treading (TT) like motion, in which the membrane preserved a fixed inclination angle with respect to the horizontal position and its steady-state shape remains indeformable. Snapshots showing the membrane deformation are provided in Fig. 2. Fig. 3 clearly shows that the area of the interior domain and the interfacial length are well preserved. In Fig. 4 (bottom), the time evolution of the inclination angle is provided and the inclination angle in the steady state is called $\theta^\star$.

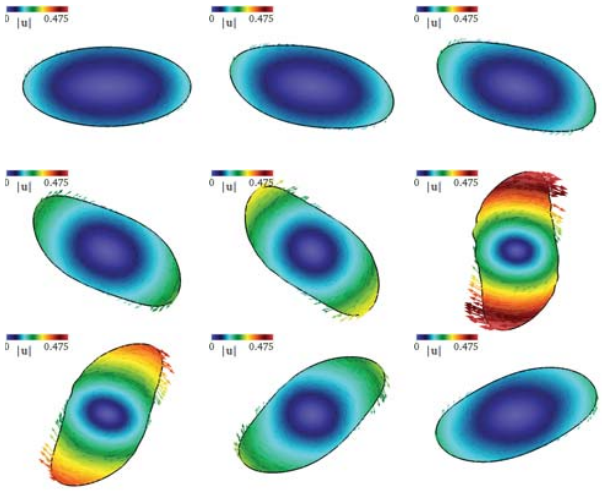

Fig. 5 Tumbling regime: Snapshots showing the dynamics of a membrane in simple shear flow (shape and velocity profile Ω) characterized by $\Xi_{2d} = 0.65$, $\mu^\star = 10$, $\mathrm{Re} = 10^{-3}$ and $\varsigma = 1/2$ at successive times $t \in \{0, 1.25, 1.75, 2.5, 3, 4.25, 4.75, 5.51, 6.5\}$, respectively

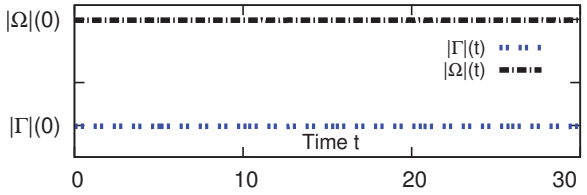

Fig. 6 Tumbling regime: Temporal evolution of the area and perimeter

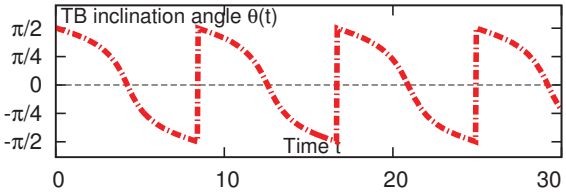

Fig. 7 Tumbling regime: Time evolution of the inclination angle

We now consider a large viscosity ratio $\mu^\star = 10$. This value is beyond a threshold value and it is known that this choice leads to a change in the membrane regime. In fact, the interior domain behaves more rigid and the membrane undergoes consequently a tumbling (TB) regime characterized by the rotation of the membrane around its center of mass. In Fig. 5, snapshots showing the tumbling dynamics and the temporal evolution of the inclination angle θ are provided. Fig. 6 depicts the good preservation of the area and membrane length during the tumbling motion. The time evolution of the inclination angle is provided in Fig. 7.

B. Validation Tests

In this section, we proceed with a numerical comparison with some available results in the published literature. We

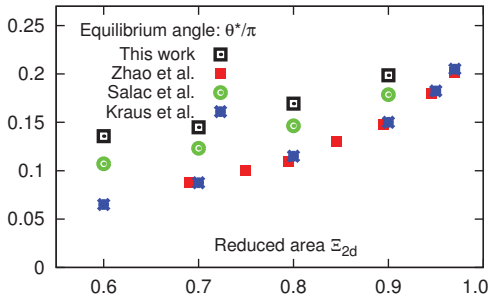

Fig. 8 Equilibrium inclination angle for membranes with different Ξ_{2d} and undergoing a TT regime, comparisons with respect to [25], [28] and [11]

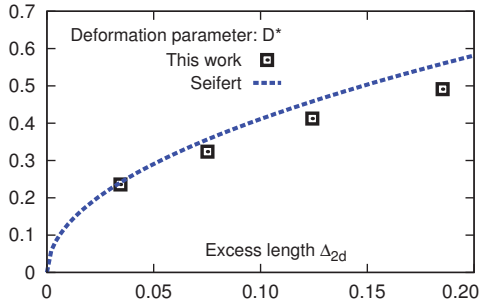

Fig. 9 The deformation parameter $D^\star$ for RBC in TT regime with respect to the excess length parameter Δ_{2d}: Comparison with model introduced by [26]

emphasize that the full expression of the Helfrich force is considered in the other works. However, the capillary number is usually considered larger that 100, which corresponds to a factor smaller 10^{-2} in front of the bending force. Accordingly, our setting corresponds to the use of too large capillary numbers. We first consider a membrane undergoing a tank treading dynamics in a simple shear flow. The physical parameters are set as follows: $\mu^\star = 1$, Re $= 10^{-3}$ and $\varsigma = 1/4$. We plot in Fig. 8 the equilibrium inclination angle with respect to the reduced area. Comparisons against some other numerical results show that a similar pattern is obtained.

We now focus on the deformation of a membrane in the steady state of a tank treading regime. The deformation parameter is evaluated by $D = (L - B)/(L + B)$, where L and B represent the major and minor semi-axes of an ellipse having the same inertia tensor as the membrane. We compare our numerical results with the prediction model introduced by Seifert [26] for vesicles undergoing a tank treading like motion. The model predicts that the deformation parameter at equilibrium $D^\star$ scales as $\sqrt{\Delta_{2d}}$. We choose the parameters $\mu^\star = 1$, Re $= 10^{-3}$ and $\varsigma = 1/4$. In Fig. 9, we plot the deformation $D^\star$ at equilibrium for several values of the shape parameter Δ_{2d}. Results show a good agreement with the theoretical prediction of Seifert [26] but with a small shifting.

Overall, although a highly simplified version of the Helfrich energy has been used, acceptable results are obtained. Indeed, the observed differences with the existing results can be explained by the use of different numerical methods, the simplified version of the bending energy, the use of different boundary conditions (periodic, Neumann, ...) and the effect of the confinement on the dynamics of the membrane.

C. Convergence Properties of the Newton Method

We proceed now with a study of the convergence properties of the Newton method. We consider several values of the time step size, and we plot the residuals' convergence curves in the semi-logarithmic scale in Fig. 10. In addition, we evaluate in Table I the order of convergence ROC of the residuals using the following expression:

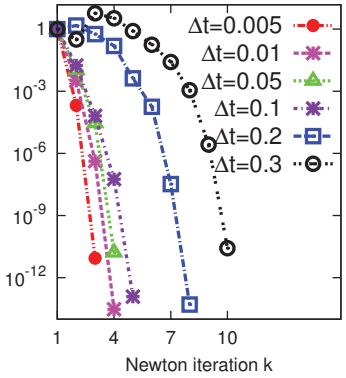

Fig. 10 Convergence curves of the residuals for several time step sizes: Results are plotted in the semi-logarithmic scale

$$\text{ROC} = \frac{\ln\left(\dfrac{|\mathscr{R}(\boldsymbol{\chi}_k^n)|_{\mathbb{V}'(\mathbf{0})}}{|\mathscr{R}(\boldsymbol{\chi}_{k-1}^n)|_{\mathbb{V}'(\mathbf{0})}}\right)}{\ln\left(\dfrac{|\mathscr{R}(\boldsymbol{\chi}_{k-1}^n)|_{\mathbb{V}'(\mathbf{0})}}{|\mathscr{R}(\boldsymbol{\chi}_{k-2}^n)|_{\mathbb{V}'(\mathbf{0})}}\right)}, \qquad \text{for } k > 2.$$

From Fig. 10 and Table I, we observe that the second-order convergence behavior is almost obtained. However, the number of iterations required to achieve the convergence increases when larger time steps are used. Indeed, the Newton strategy is known to have local convergence properties, and the algorithm only converges if the starting values are close enough to the expected solutions. When increasing Δt, the starting value becomes far from the solution and the convergence can be deteriorated if too large time steps are used. There exist several strategies in the literature that enable to address this issue, such as the initialization by a fixed point algorithm or the line search algorithm. That is beyond the scope of this work.

D. Grid Convergence

We now perform the simulation of a membrane having a reduced area $\Xi_{2d} = 0.8$ and undergoing a tank treading regime at the steady state. We study the spatial accuracy of the numerical approximations by computing normalized errors in the energy norms on successively refined meshes with respect to a highly accurate reference solution (obtained with a mesh

TABLE I
ORDERS OF CONVERGENCE OF THE RESIDUALS FOR SEVERAL VALUES OF THE TIME STEP SIZE

k	$\Delta t = 5 \times 10^{-3}$	5×10^{-2}	10^{-2}	0.1	0.2	0.3
3	2.0024	1.5497	0.4281	1.3849	2.3955	3.2582
4		1.8466	1.3017	1.2575	1.3946	0.3742
5			1.2608	1.8534	2.7267	1.0060
6					0.8732	1.0743
7					2.7319	1.2558
8					1.5564	1.6363
9						1.9303
10						1.9054

TABLE II
SPATIAL CONVERGENCE IN THE NATURAL NORMS FOR A MEMBRANE WITH $\Xi_{2d} = 0.8$ AND UNDERGOING A TANK-TREADING REGIME AT THE STEADY STATE

$1/h$	$E(\boldsymbol{u})$	ROC$_{\boldsymbol{u}}$	$E(p)$	ROC$_p$
20	1.952E-1		6.154E-1	
40	1.033E-1	0.918	1.935E-1	1.669
80	8.917E-2	1.130	9.050E-2	1.096
$1/h$	$E(\lambda)$	ROC$_\lambda$	$E(\varphi)$	ROC$_\varphi$
20	7.117E-1		9.067E-2	
40	3.205E-1	1.151	5.907E-2	0.618
80	1.695E-1	0.919	3.352E-2	0.817

size of $h = 1/160$). Let $\|\cdot\|_{0,2,\Lambda}$ and $\|\cdot\|_{1,2,\Lambda}$ design the L^2-norm and the semi-norm H^1, respectively. These errors are computed at the final time $T = 10$ when the steady regime is reached and are given by:

$$E(\boldsymbol{u}) = \frac{\|\boldsymbol{u}_h - \tilde{\boldsymbol{u}}\|_{1,2,\Lambda}}{\|\tilde{\boldsymbol{u}}\|_{1,2,\Lambda}}, \quad E(p) = \frac{\|p_h - \tilde{p}\|_{0,2,\Lambda}}{\|\tilde{p}\|_{0,2,\Lambda}},$$
$$E(\lambda) = \frac{\|\lambda_h - \tilde{\lambda}\|_{0,2,\Gamma}}{\|\tilde{\lambda}\|_{0,2,\Gamma}} \text{ and } E(\varphi) = \frac{\|\mathscr{H}_\varepsilon(\varphi_h) - \mathscr{H}_\varepsilon(\tilde{\varphi})\|_{0,2,\Lambda}}{\|\mathscr{H}_\varepsilon(\tilde{\varphi})\|_{0,2,\Lambda}}.$$

In addition, we evaluate the rate of convergence ROC with respect to the corresponding refinement level, referred to as a superscript l. It is given by:

$$\text{ROC} = \frac{\ln\left(\dfrac{E^{l-1}}{E^l}\right)}{\ln\left(\dfrac{h^{l-1}}{h^l}\right)}$$

The computed errors are reported in Table II, along with the corresponding rates of convergence. Results show that suboptimal convergence rates are obtained for the errors in $\boldsymbol{u}$, p and λ. The error $E(\varphi)$ converges with almost a linear convergence behavior.

E. Comparison with an Explicit Decoupling Scheme

We finally perform a comparative study with a fully explicit decoupling scheme, usually used in the literature for free-interface problems. The explicit method consists in decoupling and solving the fluid problem and the level equation in a segregated fashion. The velocity, pressure and surface tension are first computed by solving the fluid problem, in which the surface operators are evaluated using the level set solution at the previous time step. The level set function is advected afterwards using the computed velocity. We consider a membrane having the reduced area $\Xi_{2d} = 0.6$ and placed in a linear shear flow characterized by $\mu^\star = 1$ and $\text{Re} = 10^{-2}$. We set the confinement level to $\varsigma = 1/2$. We measure in Table III the maximum time step size allowed by both schemes. Results show that the present method allows to use significantly larger time steps compared to those allowed by the explicit method. In particular, it is possible to obtain a stable solution for time steps 45 times larger than those allowed by the explicit method.

TABLE III
EVALUATION OF THE MAXIMAL TIME STEP Δt_{MAX} ALLOWED BY THE PRESENT METHOD AND THE EXPLICIT METHOD FOR SEVERAL VALUES OF THE MESH SIZE

$1/h$	$\Delta t_{\max}$(Explicit)	$\Delta t_{\max}$(Implicit)
20	5.65×10^{-2}	0.78
40	2.40×10^{-2}	0.61
80	6.34×10^{-3}	0.17
160	1.07×10^{-4}	4.75×10^{-3}

V. CONCLUSION

In the present paper, we have introduced a fully implicit and monolithic finite element method for the numerical simulation of inextensible fluidic membranes immersed in a Newtonian fluid. The method is based on the use of the Newton method in a fully Eulerian framework. We have used a highly simplified version of the Canham-Helfrich energy, in which the bending forces and the asymmetry of the membrane and its enclosing environment are disregarded, but we have preserved the modeling of an inhomogeneous membrane tension. A consistent Newton-Raphson linearization is performed. Numerical results show that the quadratic convergence of the Newton method has been obtained. In addition, the method allows to use significantly larger time steps with respect to the fully explicit decoupling strategy.

This work is part of a larger and ongoing project aimed at modeling the dynamics of red blood cells under the effect of the full Canham-Helfrich force. Some other extensions of the present method are being currently explored. In particular, we are focusing on the development of a cubically convergent Newton variant and the construction of robust preconditioners that would allow substantial savings in computational effort.

APPENDIX A
USEFUL DERIVATIVES AND LINEARIZATION EXPRESSIONS

We consider the signed distance assumption resulting from the resolution until convergence of the redistancing problem. In this Appendix, we provide the directional derivatives of some quantities in the direction of the increment $\delta\boldsymbol{\chi}$.

$$D\boldsymbol{n}[\delta\boldsymbol{\chi}] = D\boldsymbol{\nabla}\varphi[\delta\varphi] = \boldsymbol{\nabla}\delta\varphi,$$
$$DH[\delta\boldsymbol{\chi}] = D\,\text{div}\,\boldsymbol{n}[\delta\varphi] = D\Delta\varphi[\delta\varphi] = \Delta\delta\varphi.$$

The linearization of the global viscosity function reads:

$$D\mu_\varepsilon(\varphi)[\delta\boldsymbol{\chi}] = (\mu^\star - 1)\delta_\varepsilon(\varphi)\delta\varphi.$$

The linearization of the term evolving the membrane tension in the momentum equation reads:

$$\begin{aligned} D\lambda\,\delta_\varepsilon(\varphi)\,\mathrm{div}_s\,\boldsymbol{v}[\delta\boldsymbol{\chi}] &= D\lambda\,[\mathrm{div}\,\boldsymbol{v} - (\boldsymbol{n}\cdot\boldsymbol{\nabla}\boldsymbol{v})\cdot\boldsymbol{n}]\,\delta_\varepsilon(\varphi)\,[\delta\boldsymbol{\chi}] \\ &= \delta\lambda\,\delta_\varepsilon(\varphi)\,\mathrm{div}_s\,\boldsymbol{v} + \lambda\,\delta'_\varepsilon(\varphi)\,\delta\varphi\,\mathrm{div}_s\,\boldsymbol{v} \\ &\quad - \lambda\Big((\boldsymbol{\nabla}\delta\varphi\cdot\boldsymbol{\nabla}\boldsymbol{v})\cdot\boldsymbol{\nabla}\varphi + (\boldsymbol{\nabla}\varphi\cdot\boldsymbol{\nabla}\boldsymbol{v})\cdot\boldsymbol{\nabla}\delta\varphi\Big)\,\delta_\varepsilon(\varphi). \end{aligned}$$

The linearization of the regularized inextensibility constraint reads:

$$\begin{aligned} D\,\delta_\varepsilon(\varphi)\,\mathrm{div}_s\,\boldsymbol{u}[\delta\boldsymbol{\chi}] &= D\,[\mathrm{div}\,\boldsymbol{u} - (\boldsymbol{n}\cdot\boldsymbol{\nabla}\boldsymbol{u})\cdot\boldsymbol{n}]\;\delta_\varepsilon(\varphi)\,[\delta\boldsymbol{\chi}] \\ &= \delta_\varepsilon(\varphi)\,\mathrm{div}_s\,\delta\boldsymbol{u} + \delta'_\varepsilon(\varphi)\,\delta\varphi\;\mathrm{div}_s\,\boldsymbol{u} \\ &\quad - \Big((\boldsymbol{\nabla}\delta\varphi\cdot\boldsymbol{\nabla}\boldsymbol{u})\cdot\boldsymbol{\nabla}\varphi + (\boldsymbol{\nabla}\varphi\cdot\boldsymbol{\nabla}\boldsymbol{u})\cdot\boldsymbol{\nabla}\delta\varphi\Big)\,\delta_\varepsilon(\varphi). \end{aligned}$$

ACKNOWLEDGMENT

The author gratefully acknowledge the financial support by the Swiss National Science Foundation through the grant 320030-149567.

REFERENCES

[1] P.R. Amestoy and I.S. Duff and J. Koster and J.-Y. L'Excellent, *A Fully Asynchronous Multifrontal Solver Using Distributed Dynamic Scheduling*, SIAM J. Matrix Anal. Appl., 2001, 23(1):15-41.
[2] J.W. Barrett, H. Garcke and R. Nürnberg, *Finite element approximation for the dynamics of asymmetric fluidic biomembranes*, preprint No. 03/2015, University Regensburg, Germany (2015).
[3] J.W. Barrett, H. Garcke and R. Nürnberg, *Stable finite element approximations of two-phase flow with soluble surfactant*, J. Comput. Phys., 297 (2015), pp. 530–564
[4] T. Biben, K. Kassner and C. Misbah, *Phase-field approach to three-dimensional vesicle dynamics*, Phys. Rev. E. 2005;72:049121.
[5] F. BREZZI AND M. FORTIN, *Mixed and hybrid finite element methods*, Springer New York, 15 (1991).
[6] P.B. Canham, *The minimum energy of bending as a possible explanation of the biconcave shape of the human red blood cell*, J. Theor. Biol., 26 (1970), pp. 61–81
[7] H. Deuling and W. Helfrich, *The curvature elasticity of fluid membranes: a catalogue of vesicle shapes*, J. Phys. 1976;37:1335–45.
[8] C. Geuzaine and J.-F. Remacle, *Gmsh: A 3-D finite element mesh generator with built-in pre- and post-processing facilities*, Int. J. Numer. Meth. Engng., 2009, 79: 1309-1331.
[9] W. Helfrich, *Elastic properties of lipid bilayers: theory and possible experiments*, Z. Naturforsch, 1973;28c:693–703.
[10] S. Hysing, *A new implicit surface tension implementation for interfacial flows*, Int. J. Numer. Methods Fluids, 51 (6) (2006), pp. 659–672
[11] M. Kraus, W. Wintz, U. Seifert and R. Lipowsky, *Fluid vesicles in shear flow*, Phys. Rev. Lett. 77 (1996) 3685–3688.
[12] Y. Kim and M.-C. Lai, *Simulating the dynamics of inextensible vesicles by the penalty immersed boundary method*, J. Comput. Phys., 229 (12) (2010), pp. 4840–4853
[13] A. Laadhari, C. Misbah and P. Saramito, *On the equilibrium equation for a generalized biological membrane energy by using a shape optimization approach*, Physica D: Nonlinear Phenomena 239 (2010) 1567–1572.
[14] A. Laadhari, R. Ruiz-Baier and A. Quarteroni, *Fully Eulerian finite element approximation of a fluid-structure interaction problem in cardiac cells*, Int. J. Numer. Meth. Engng. 96 (2013) 712–738.
[15] A. Laadhari, P. Saramito and C. Misbah, *An adaptive finite element method for the modeling of the equilibrium of red blood cells*, Int. J. Numer. Meth. Fluids 80 (2016) 397–428.
[16] A. Laadhari, P. Saramito and C. Misbah, *Computing the dynamics of biomembranes by combining conservative level set and adaptive finite element methods*, J. Comput. Phys. 263 (2014) 328–352.
[17] J. Lowengrub, J-J. Xu and A. Voigt, *Surface phase separation and flow in a simple model of multicomponent drops and vesicles*, Fluid Dyn. Mater. Proc. 2007;3(1):1–19.
[18] J. Katsaras and T. Gutberlet T, *Lipid bilayers: structure and interactions*, Springer-Verlag, Berlin, 2001.
[19] M.P.I. Forum, *MPI: A Message-Passing Interface Standard*, http://www.mpi-forum.org (Accessed: 28.11.2016).
[20] MUMPS: MUltifrontal Massively Parallel Solver, http://mumps.enseeiht.fr/index.php (Accessed: 28.11.2016).
[21] S. Osher and J.A. Sethian *Fronts propagating with curvature-dependent speed: Algorithms based on Hamilton-Jacobi formulations*, J. Comput. Phys., 79 (1) (1988), pp. 12–49.
[22] Paraview: Parallel visualization application, http://paraview.org (Accessed: 28.11.2016).
[23] P. Saramito, *Efficient C++ finite element computing with Rheolef*, CNRS-CCSD ed., 2013. http://www-ljk.imag.fr/membres/Pierre.Saramito/rheolef/rheolef-refman.pdf (Accessed: 22.09.16).
[24] D. Salac and M. Miksis, *A level set projection model of lipid vesicles in general flows*, J. Comput. Phys., 230 (2011), pp. 8192–8215
[25] D. Salac and M. Miksis , *Reynolds number effects on lipid vesicles*, J. Fluid Mech. 711 (2012) 122–146.
[26] U. Seifert, *Configurations of fluid membranes and vesicles*, Adv. Phys. 46 (1997) 13–137.
[27] T. Williams and C. Kelley, *Gnuplot: An Interactive Plotting Program* http://www.gnuplot.info (Accessed: 28.11.2016).
[28] H. Zhao and E. S. G. Shaqfeh , *The dynamics of a vesicle in simple shear flow*, J. Fluid Mech. 674 (2011) 578–604.

Aymen Laadhari received the Engineering degree from Tunisia Polytechnic School, Tunisia, in 2006. He received the Ph.D. degree in Applied Mathematics from Grenoble University, France, in 2011. He was a scientific collaborator with the Mathematics Institute of Computational Science and Engineering at the École Polytechnique Fédérale de Lausanne (Swiss Federal Institute of Technology Lausanne), Switzerland. He is currently a researcher with the Swiss Federal Institute of Technology Zürich, Switzerland. His current research interests include mathematical modeling and software development of new computational methods for the simulation of biomedical phenomena.